Acta of Bioengineering and Biomechanics
Vol. 17, No. 3, 2015

Original paper
DOI: 10.5277/ABB-00165-2014-02

BoneCreo: a novel approach for generating a geometric model of the bone structure

ARTUR WRONA*

Institute of Biomedical Engineering and Instrumentation, Wrocław University of Technology, Wrocław, Poland.

Bones, the fundamental part of the skeleton, are constantly subjected to many biological processes including growth, feeding and remodelling. Remodelling causes changes in bone structure that may be difficult to notice on a day-to-day basis but become significant over the longer time span. It acts on the cancellous and cortical bone tissue, causing alterations in thickness and spatial arrangement in the first and alternations in pore size in the second. In healthy individuals such changes are a part of the natural bone remodelling process explained by Wolff's law. However, the direction of such changes is difficult to predict in patients in various pathological states in which bone health is affected. Here, we present a method to generate a computer based geometric model of the bone structure based on the cancellous tissue structure images. As a result we obtained a geometric model of the structure corresponding to the physical model of the cancellous bone. Such a model can be used in computer simulation to predict the remodelling changes in the healthy and pathological bone structures.

Key words: *numerical model, bone tissue, image analysis, computer simulation*

1. Introduction

The alterations in the bone structure due to the remodelling process are of major concern in implantology and dentistry, where metal elements need to be surgically and permanently inserted to the bone to bring functional rehabilitation [3], [9], [14], [25]. Computer simulations of the bone structure have proven to be a useful way of assessing its behaviour before and after such surgical interventions [2], [7], [12], [21]. However, these require a valid model of the bone structure in question for the simulation results to be applicable to the real-case and/or patient-based scenarios. This remains the biggest challenge since the irregular structure of the cortical bone tissue cannot be easily described by mathematical equations.

The typical histomorphometric studies provide a set of descriptive measurements of the cortical bone structure including trabecular thickness (*Tb.Th*), trabecular number (*Tb.N*) and trabecular pore size (*Tb.S*) in the area examined as well as bone density in the cross-sectional area [8], [18], [24]. These describe the average mechanical and spatial properties of the bone structure and as such cannot be directly used to build a bone structure model to be used for computer simulation, e.g., by the Finite Element Method (FEM) [4], [9], [22], [23]. In FEM, bone models are typically based on the density distribution of the cancellous tissue (using the cross-sections of the bone tissue from the micro-CT images) and include Young's modulus and Poisson's ratio [9], [17]. FEM simulations allow investigating the changes in the bone structure (density, displacements) that are in the same directions as the changes undergoing in the healthy bone.

Using the density approach, an accurate three-dimensional geometric model of the bone structure can be developed based on the two-dimensional micro-CT images [5], [14], [18]. Here, the design is based on the high number of voxels that can go as high as millions depending on the size of the sample. As a consequence, the computer simulations based on

* Corresponding author: Artur Wrona, Institute of Biomedical Engineering and Instrumentation, Wrocław University of Technology, Wybrzeże Stanisława Wyspiańskiego 27, 50-370 Wrocław, Poland. Tel: +48 71 320 39 74, e-mail: artur.wrona@pwr.wroc.pl
Received: August 26th, 2014
Accepted for publication: October 21st, 2014

high in voxels models are time-consuming and require large computing power.

The main aim of the article is to present and evaluate the developed method of generating a geometric model of trabecular bone. This model should be based on photographs of the cross section of the spongy bone tissue. The geometrical model obtained should be as simple as possible and reflect the bone structure. The underlying assumption of the model is that it is generated with the minimum number of components to facilitate the subsequent simulation of the system (which should reduce computational time and computer power required).

In computer modelling it is important to verify theoretical results with experimental data. Here, we will compare the results obtained by our model with the results of the uniaxial compression of the physical model.

2. Material and methods

Briefly, the proposed approach is based on series of image processing steps as well as optimization steps to find a simple yet powerful model of the bone structure. The input of the algorithm is an image file showing a cross-section of the bone structure. The output constitutes the coordinates of geometric model and information about trabecular like thickness and moment of inertia and they are save to the text file. The development of the algorithm was based on the physical model of the bone structure (snapshot) and its testing was based on the comparison of the computer simulation of the generated model with experimental results obtained on the physical model (uniaxial load testing) described here. The algorithm was implemented under MATALB ver. 7.5 environment with basic toolbox for digital image processing and is fully described in Section 2.1 BoneCreo method. The Matlab code is available on request: artur.wrona@pwr.edu.pl

2.1. BoneCreo method

The steps of the BoneCreo algorithm are shown in a flowchart in Fig. 1. The first part is based on the user-driven optimization methods and includes input, filtering & borders extractions and nodes determination procedures. The second part uses fully automated procedures of finding connections between nodes, determining the diameters of sections and saving the output (Fig. 2).

2.1.1. Input

The input of the algorithm is an image file showing a snapshot or cross-section of the bone structure. The only condition is that such image should show a clear structure of trabecular bone obtained using the microtomography technique or with an optical microscope. Preferred image formats are .bmp, .png. or .jpg. This is important because user should be able to perform

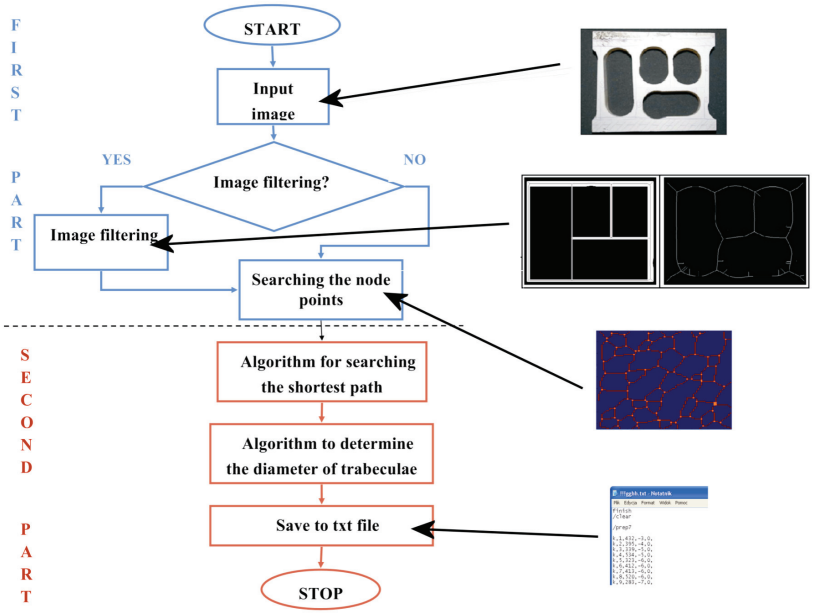

Fig. 1. Block diagram showing the operations of the own program;
on the right there are pictures ilustrating the results of the various stages of the algorithm

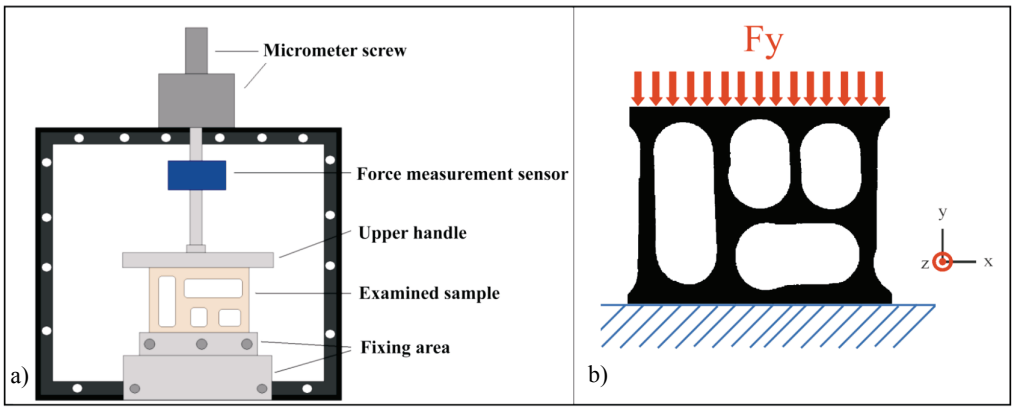

Fig. 2. Measuring stand for investigations of physical model displacement using the method of electronical speckle pattern interferometry: (a) fixing system, (b) schematic model with marked boundary conditions – the force and points of support

digital image processing by using another program. MATLAB ver. 7.5 has the ability to read also other image formats such as .tiff, .giff, .pgm or .pbm.

2.1.2. Filtering and borders extractions

Filtering is applied to remove noise and interference that appears during taking the picture of the bone structure, either the model one or during medical examinations. Examples of such disturbances can be of various kind like: random variation of brightness or colour information, salt-and-pepper noise, shot noise or Gaussian noise. This part of the algorithm is based on simple image processing tools available in MATLAB ver. 7.5 environment that include averaging pixel values, sharpening, smoothing and conversion of an RGB image to a grey scale. The algorithms behind these methods are well established, e.g., the Otsu method, thresholding or image binarization [6], [11], [15], [19]. In addition, picture is converted to binary form and all the subsequent steps are based on binary image processing. Here, the user selects the adequate filtering methods and the amount of repetition (user-based optimisation) since the quality of the filtered image is best assessed by the user.

Based on the filtered image, the object's (bone structure) borders (inner and outer) are extracted using the morphological operations, in particular, by removing pixels on the boundaries of the object but not allowing objects to break apart, thus resulting in the image skeleton (function *bwmorph*, settings *skel*) (Fig. 3). The common issue with this function is adding short fragments (or branches) to the object's boarders. Here, such side effect of obtaining a skeleton procedure would affect the structure of the obtained bone structure, in particularly affecting the trabeculae (numbers and dimensions). To address this issue, the pruning operation (function *bwmorpth*, settings *spur*) designed for this purpose is applied. Again, the number of repetitions is left to the user, as it is difficult to predict the amount and size of the extra branches/boarders artefacts in the skeletonized image.

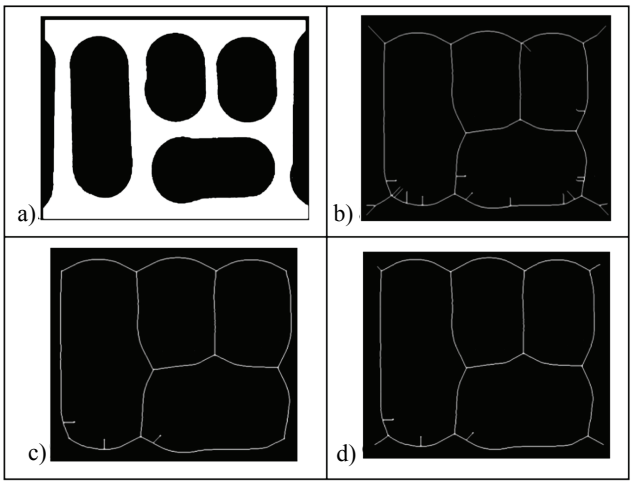

Fig. 3. Examples of skeleton (b) and pruning process with different iterations (c), (d)

In addition, a procedure to account for the "surface size" bias was implemented. It was noticed that the smaller objects (smaller surface) gave higher quality (defined as the ratio of the number of added branches (artefacts) to all line borders) skeletonized images (Fig. 4a). Here, first the borders between the object and the background are found and the pixel coordinates of the borders are stored. In the next step the program removed, as set by the user, a fragment of pixels forming an object–background border. This procedure allowed the total area of the object to be reduced. Changing the dimensions of the inner surfaces between the trabeculae (included in the surface of the object) was also possible to control by the user (Fig. 4b–d). The procedures in this case were the same as the smoothing of the shapes on the object–

background border. This was possible because the inner borders of the object are determined. Finally, a smoothing function is applied to the borders (irregular shape) and the binary picture with clearly marked object's (bone structure) borders (enhanced boarders as compared to the input image) is obtained. The user's control of the filtering and skeletonization processes ensures the maintenance of border continuity.

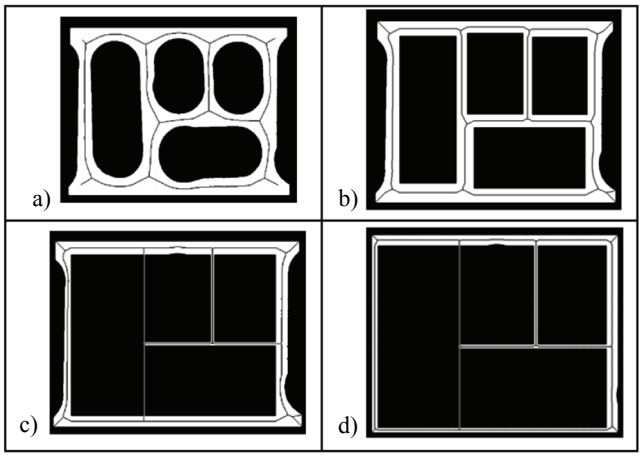

Fig. 4. Diagrams showing the application of skeleton of the physical model, taking into account changes in the surface of the object. (a) Skeleton of the model without changing the surface (b)–(d) Different variants of the surface changes with superimposed skeleton

2.1.3. Node determination

Nodes are defined as the points where three or greater part of the skeleton (borders) intersect and are obtained based on the skeletonized image obtained as described above and the application of so called masks. Masks, in image processing, are images of the same dimension as the original image or the region of interest (here, 3 × 3 pixels) that are used to restrict the operations to the selected part of the image (to the selected pixels). Each element in the mask represents a value assigned to the corresponding pixels. To identify the object nodes, five masks were selected based on the analysis of the skeletonized images (Fig. 5a).

The pixels that are adjacent to at least three other pixels belonging to the skeleton are found and highlighted by assigning a value of 50. These pixels are compared with the five masks (scanning process). If the two surfaces (skeleton's region and the mask) match, the central pixel corresponding to the node is selected and assigned a value of 100. The coordinates of the node pixels are in a separate matrix. The remaining pixels are treated as the set of the pixels adjacent to the nodes pixels (Fig. 5b).

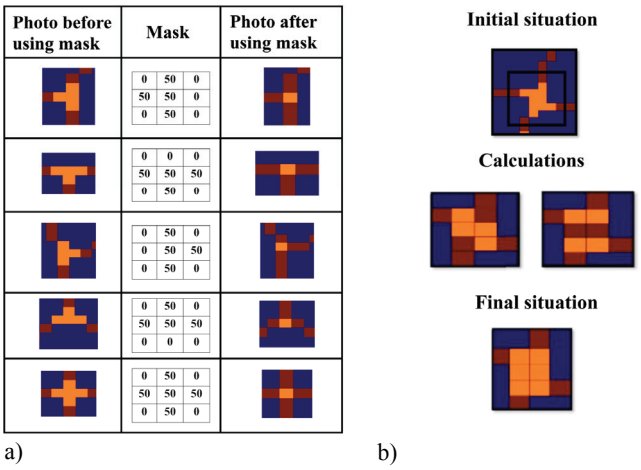

Fig. 5. (a) Table showing the main types of standard masks and their application. (b) Example of custom masks application

2.1.4. Finding connections between the nodes

The connections between the nodes are found using the algorithms solving a shortest-path problem for a graph, in particular Dijkstra's algorithm and A* search algorithm [11], [15]. In the first step, the matrix representing the image of the skeleton (pixel assigned values of 1) and the matrix representing the nodes (pixels values of 100) are superimposed. Next, due to different values assigned to skeleton pixels and nodal pixel, all the proximal pixels connected to the nodes can be identified. Each node is surrounded by eight neighbouring pixels of values either 0 or 1. The coordinates of value 1 pixels are stored and in the next step these pixels become the central pixels for the 3 × 3 matrix. The process iterates until the selected matrix contains a nodal pixel. The free ends (lack of the nodal point) are not supported by this approach. Therefore, in such case only the coordinates of the staring nodal pixel and the coordinates of the final pixels are saved.

2.1.5. Determining the diameters of sections

Trabecular thickness (Tb.Th) is calculated by adding three matrices representing (i) image after the filtration with the selected object (pixel values set to 1, pixel background values set to 0), (ii) skeleton of the object (pixel values set to 6), and (iii) nodal points (pixel values set to 1). These matrices and information about pixel coordinates forming the section allow a pixel to be set for which thickness of section will be calculated. During this procedure, it is also determined that the angle of inclination of the trabecular is relative to the axis OX.

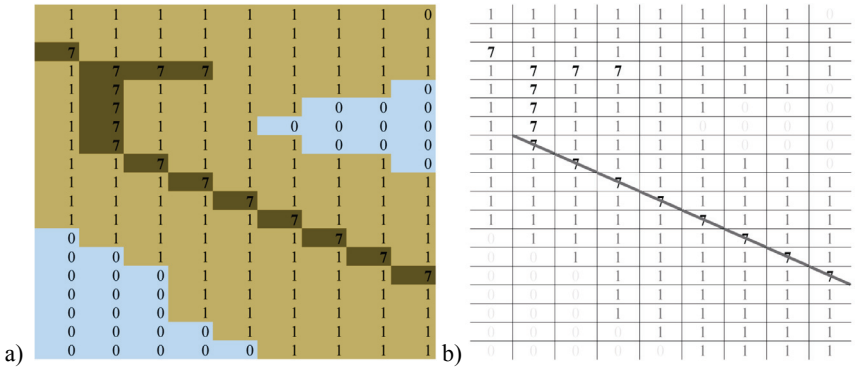

Fig. 6. Diagram showing the method of determining the thickness of trabecular bone. (a) A fragment of a matrix with marked area of trabecular bone (value 1), the skeleton (value 7) and background (value 0); (b) a line defining the trabecular orientation, which is the basis for finding pixels with a value of 1 situated perpendicular to this line

The value of this angle indicates the direction of the trabecular. Furthermore, it is also used to calculate the thickness of the trabecular.

Trabecular thickness value was calculated for the central pixel of the section. The thickness is determined as a sum of the neighbouring pixel arranged linearly, perpendicular to the skeleton (skeleton pixels had a value equal to 7) and having a value of 1, see Fig. 6.

Description	Name	Formula
Cross-sectional area	AREA	$B \cdot H$
Area moment of inertia	JZZ	$\frac{(B \cdot (H^3))}{12}$
Area moment of inertia	JYY	$\frac{(H \cdot (B^3))}{12}$
Thickness along Z axis	TKZ	B
Thickness along Y axis	TKY	H
Orientation about X axis	THETA	0
Initial strain	ISTRN	0
Torsional moment of inertia	IXX	$\left(\frac{B \cdot H}{3}\right) \cdot (B^2 + H^2)$
Shear deflection constant Z	SHEARZ	$\frac{6}{5}$
Shear deflection constant Y	SHEARY	$\frac{6}{5}$

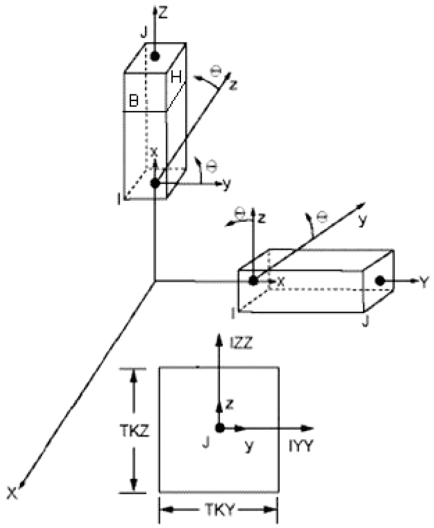

Fig. 7. The parameters describing the material properties of trabecular used in computer simulation

Thickness of each section allows the parameters characterizing element of beam type to be calculated. This is one of the basic types of elements available in the program ANSYS 11. It is described by several parameters defining the properties of the material, for example: area moment of inertia for each axis and torsional moment of inertia. The appropriate equations for these and other parameters, such as the shear deflection constant Z and Y, cross-sectional area and thickness along Z axis and Y axis are given in Fig. 7.

In the course of determining the diameters of thickness user has the possibility to split sections, representing the trabecular, to shorter ones. This operation, in the course of future research, increases accuracy of calculation of the trabecular thickness and also increases the complexity of the model and the calculation time during computer simulation.

2.1.6. Output

The obtained geometrical model of the bone structure is save to a text file. This file inside includes information on: the coordinates of the nodes, connections between the respective nodes and information on the material properties of each segment. Information about the boundary conditions should be introduced by the user in the appropriate program for computer simulation. Thus, prepared text file can be directly used as in input file for ANSYS, i.e., for the subsequent computer simulation of the behaviour of the object with the Finite Element Method.

2.2. Physical model of the bone structure

The physical model of the cancellous bone structure was made of epoxy resin. The physio-chemical

properties of the epoxy resin (Young's modulus – 20 000 MPa, Poisson's ratio – 0.4) make it an adequate material to produce model fragments of the human skeleton, including bones (femur, tibia) and vertebrae. The values of Young's modulus and Poisson's ratio allow assuming that the epoxy resin bones mimic well the human bones under experimental conditions. The physical model did not include bone marrow as the bone marrow is mainly involved in the feeding processes and does not affect largely the remodelling processes. The model was made on the milling machine by cutting four holes from the piece of epoxy resin measuring 61 × 51 × 7 mm resulting in six sections corresponding to the trabecular bone and empty spaces representing pores in the spongy tissue (Fig. 8a). The model included two handing elements for fixing the model to the testing bench during experiments (Fig. 8b).

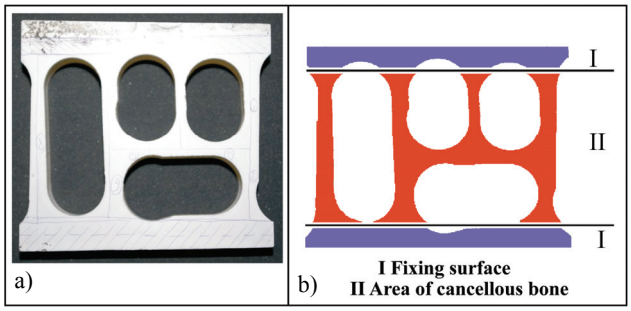

Fig. 8. Physical model of cancellous bone (a) with separated area of cancellous bone and two fixing surfaces (b)

2.3. Experimental methods

The physical model was subjected to the uniaxial load test and results recorded using Electronic Speckle Pattern Interferometry (ESPI) method that uses the ability of laser to interfere to determine the values of the displacements in the objects. ESPI was chosen due to its non-invasive approach and high accuracy. The ESPI does not cause any permanent deformation to the testing material, thus allowing a vast scope of the measurement to be obtained by repeating the load test. In addition, it allowed capturing the results of the small displacements (order of 0.1 mm), with the bone tissue being quite vulnerable (the average of the compressive strength of 150 MPa and strongly dependent on anatomic location [10]). The forces of the load could not exceed a single Newton and the approach of the small increments of the force had to be chosen.

The measuring stand and the system are shown in Fig. 2. The distance between the sample and the camera head was measured from the end of the lens to the attachment of the sample and was equal to 25 cm. The fixing system for the sample was made of metal frames with the plastic elements, which protected the sample from moving during the load test. The value of the force was adjusted by micrometre screw combined with a sensor to measure the electrical voltage.

During one measurement the sample was loaded twice. The first load (so-called initial load) was designed to stabilize the sample, except that there was also recorded by the CCD camera the image showing the distribution of spots on the surface of the physical model. During the second load value of the force was increased by 6 N, and then re-recorded spot-on the surface of the model. As a result of the interference of both holographic images a band pattern was obtained, which was later converted to a digital signal and treated by the software included with the CCD camera Istra Etemeyer, in order to determine the displacement map observed on the surface of the physical model. Sample displacement map obtained in the studies is

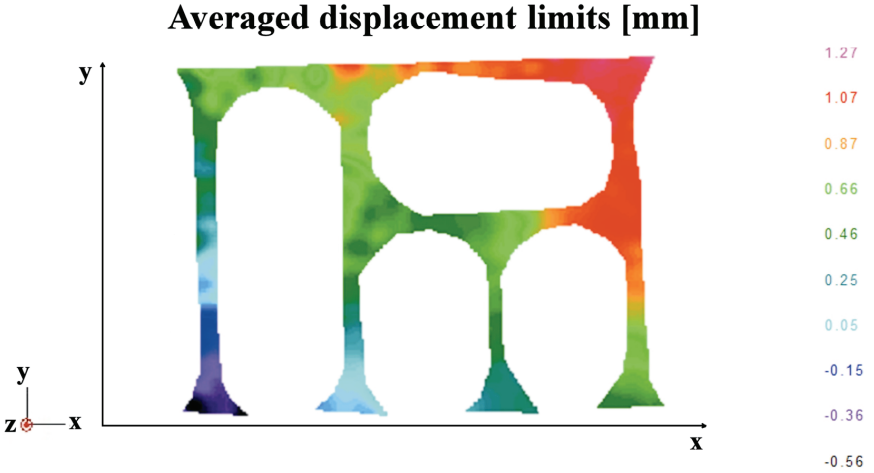

Fig. 9. Displacement maps of physical model cross section in direction of *OY* axis (vertical axis)

shown in Fig. 9. This procedure was repeated for the forces equal 83 N, 235 N and 382 N. The increase in the value of the load caused expansion of the area with the highest average displacements (upper right corner of the model in Fig. 9).

2.4. Computer simulations

The computer simulations of the behaviour of generated model in uniaxial compression were run in ANSYS11. Two surfaces representing the fixing elements were added in the form of a rectangular area, i.e., a grid system composed of 8 nodes with 2 degrees of freedom. The final geometric system, including the fixing surfaces, was thereafter made up of 3900 elements and 8157 nodes. The perfectly linear elastic material with linear stress-strain characteristics was chosen for the system. The elastics modulus was 20 000 MPa and the value of Poisson's ratio was 0.3. To mimic the experimental load test, the force along *OY*-axis was applied (Fig. 2b).

3. Results

The approach of generating the model was verified by comparing the properties (static and dynamic) of the generated model to those of the physical model. The dimensions and the structure of the generated model were calculated using pixel counts (pixel resolution), converted to mm (400 pixels corresponded to 40 mm) and compared to the measurements of the physical model (calliper measurements, 0.01 mm resolution). The model measurements were in line with the physical model dimensions, i.e., the length of width of the model A′ = 39.8 mm, the height B′ – 38.5

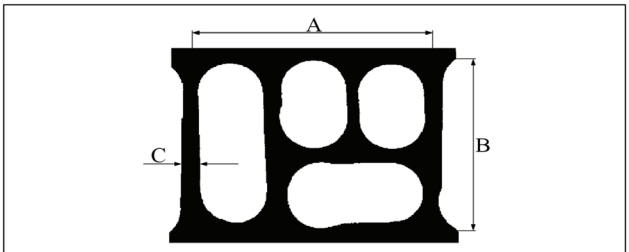

	Real dimension [mm]	Dimension calculated by the own program [mm]
A- length	40 +/- 1	39.8*
B - height	40 +/- 1	39.5*
C - diameter	24 +/- 1	22*

Fig. 10. The values of the dimensions of the physical model from the operation of the own program (* length obtained by calculating the number of pixels)

were within the measurement errors of the physical model (A = 40 ± 1 mm, B = 40 ± 1 mm), whereas the trabecular diameter was C′ = 22 mm, just 1 mm off the physical model C = 24 ± 1 mm, constituting only a small error, less than 10% (Fig. 10). In addition, the agreement between the generated and the physical model can be observed when visualizing the generated model in ANSYS (Fig. 11). Only a slight, but expected difference near the fixing regions was noticed as these were modelled in a simplified way (by adding two rectangular areas) as compared to the physical model (Fig. 12).

The dynamic properties of the generated model were examined in the computer simulations of the uniaxial compression (in ANSYS) and compared to the experimental results carried out on the physical model. The displacement profiles for the selected points along the *OY* axis were alike for the generated model (computer simulations) and the experimental test (physical model, Fig. 13). The slope values for both fitted regression lines (generated and physical model) were not significantly different (Student's *t*-test), thus confirming that dynamic properties of the

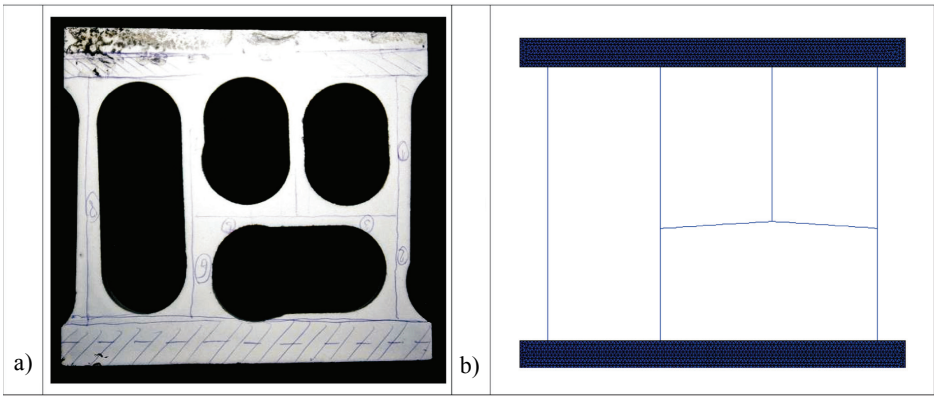

Fig. 11. The physical model used in experimental research (a) and the geometric model (b) obtained through the use of the own program

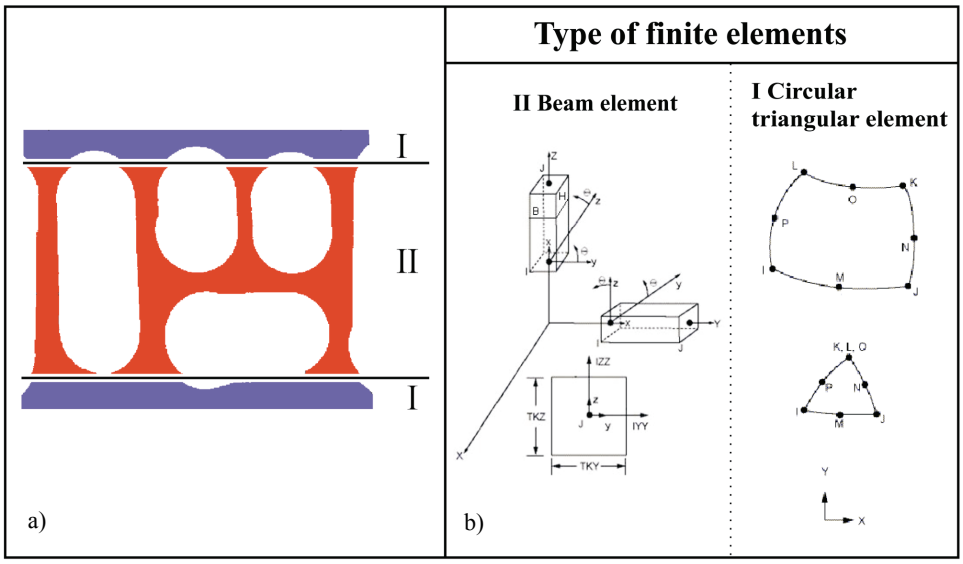

Fig. 12. The division of the physical model to fixing elements (a) and the trabeculae. Next to the physical model are shown the types of the finite element used to apply for each of the surfaces (I – circular triangular elements, II – beam elements)

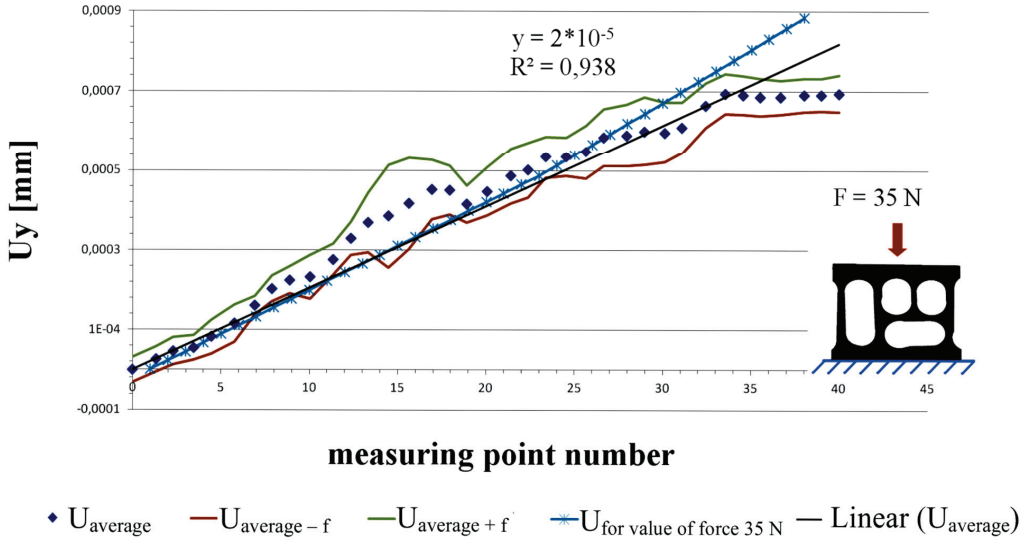

Fig. 13. Distribution of displacement of physical model cross section along vertical axis of symmetry in experimental study for the selected measurement points (red line – average displacement minus stand. dev.; green line – average displacement plus stand. dev.; blue point – average displacement) and for computer simulation for the selected measurement points (light blue line – displacement for value of force 35 N); f means standard deviation calculated for all points in the experimental study

physical model were accurately reflected in the generated model.

4. Discussion

The modern development of technology allows the geometry of the bone tissue to be mapped with very high precision, distinguishing both types of tissue – cancellous and cortical bone. The resulting image can be use din computer simulations of various kinds of issues, such as assessment of the shape of the stabilizers in the process of regeneration of bone fracture, investigation of the correlation between the tissue and implant in bone remodeling process or in dentistry to evaluate the treatment process after a fracture of the mandible [13], [20]. One of the many tools to solve the problems described is a specialized software such as SIMPLEWAWE, ImageJ or CellProfiler [26]. These programs allow us to get information about the parameters of bone structure used later in histomorphometric studies, as well as to generate complex three-dimensional images of bone structure [1], [17]. The ability to reproduce a large and complex structure entails the use of computers for supercomputing. In

addition, one should remember that with the increase of the test fragment of the bone the size of the output files is rapidly increasing.

Here, we have introduced a novel approach to generate a geometrical model of the bone structure based on its image that is design to be used as the input file in computer simulations to study its behaviour in ANSYS program. The approach was developed and successfully tested on the physical model of the bone structure, allowing obtaining similar profiles of displacements in the uniaxial compression. There is also possibility of implementing other types of compression and add them to the generated model.

The author showed that the quality of the generated model depends largely of the image processing steps used in the approach, and hence part of such a method is based on the quality control as carried out by the user. Other parts are fully automated.

The final geometric model does not differ in the shape of the actual object and the maximum difference of dimensions does not exceed 10% (Fig. 11). This discrepancy does not significantly affect the final results of the study, whose aim was to verify the behavior of the virtual physical model of bone tissue of experimental research model under compressive force. The differences between the plots – Linear and $U_{\text{for value of force 35 N}}$ in Fig. 13, may result from the adopted simplified model and the application of a uniform material with average material properties.

Geometric model, prepared according to the procedure described in the article (Fig. 14), can be used in various kinds of tests with the bone material, wherein as the final result important is the shape of the bone structure and the degree of its deformation. Principal example of such research is to analyze the process of functional adaptation or evaluation of behavior in the environment of bone prosthesis after surgery arthroplasty [16].

As the next step we will adopt the present algorithm to three dimensional space, which will increase the time of calculations. A comparison of the results obtained by two and three dimensional models should allow us to estimate the meaning of the two dimensional approximation. In extreme cases such simplification can lead to significant differences in the distribution of the deformation at the surface of the model and real object. The differences described also appeared in the present paper. The scale of them was not large as evidenced by little change in the graph (in Fig. 13, the difference between the experimental linear line (Linear) and the line obtained by computer simulation – $U_{\text{for value of force 35 N}}$).

Future modeling should also include both types of the tissue – cancellous and compact bone. According to the literature, each of these types of tissue contributes significantly to the process of remodeling shaping the architecture of the trabecular bone commonly known as the process of functional adaptation of bone tissue [27], [28].

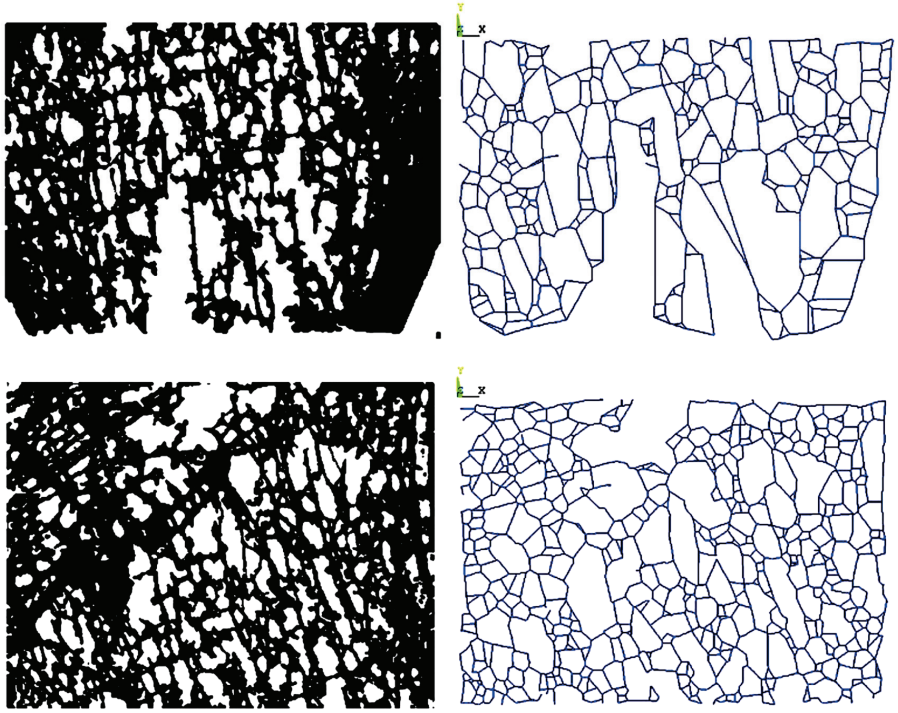

Fig. 14. Exemplary models of geometric images derived from cancellous bone fragments of proximal tibial epiphysis

Ultimately, the program should allow for the transfer of the bone structure to the virtual space simulation program, in order to assess the impact of the interaction between bone and metal element such as endoprosthesis of the hip.

The obtained theoretical results discussed here were compared with the results of the experiments performed on the own physical model. Because the main aim of this paper is evaluation of the algorithm of creation of geometrical model that is why we did not compare our results with other literature models.

Acknowledgements

The author would like to thank Krzysztof Ścigała for his help and valuable advice during the research which significantly contributed to the completion of the project. All tests were performed in the Division of Biomedical Engineering and Experimental Mechanics of Wrocław University of Technology.

References

[1] AARON J.E., MAKINS N.B., SAGREIYA K., *The Microanatomy of Trabecular Bone Loss in Normal Aging Men and Women*, Clin. Orthop. Relat. Res., 1987, Vol. 215, 260–271.

[2] AMBROSI D., ATESHIAN G.A., ARRUDA E.M., COWIN S.C., DUMAIS J., GORIELY A., HOLZAPFEL G.A., HUMPHREY J.D., KEMKEMER R., KUHL E., OLBERDING J.E., TABER L.A., GARIKIPATI K., *Perspectives on biological growth and remodeling*, J. Mech. Phys. Solids, 2011, Vol. 59(4), 863–883.

[3] BĘDZIŃSKI R., ŚCIGAŁA K., *Biomechanical basis of tissue – implant interactions*, Computer Methods in Mechanics CMM; Series: Advanced Structured Materials, 2009, Vol. 1, 379–390.

[4] BOUTROY S., VAN RIETBERGEN B., SORNAY-RENDU E., MUNOZ F., BOUXSEIN M., DELMAS P., *Finite Element Analyses Based on In Vivo HR-pQCT Images of the Distal Radius is Associated with Wrist Fracture in Postmenopausal Women*, J. Bone Min. Res., 2008, Vol. 23, 392–399.

[5] WANG C., ZHANG C., WU H., DONG X., *Bone Adaptation Model Combined Micro-Modeling and Remodeling Processes*, Bioinformatics and Biomedical Engineering, 2011, Vol. 1–4. DOI: 10.1109/icbbe.2011.5780457.

[6] CIACH-ŻELAZKO A., TOKARCZYK R., *Korekcja obrazów cyfrowych dla optymalizacji ich automatycznego pomiaru*, Archiwum Fotogrametrii, Kartografii i Teledetekcji, 2004, Vol. 14, 1–13.

[7] FERNANDES P.R., FOLGADO J., JACOBS C., PELLEGRINI V., *A contact model with in growth control for bone remodelling around cement less stems*, J. Biomech., 2002, Vol. 35(2), 167–76.

[8] GAGNÉ P., MEUNIER J., STE-MARIE L.-G., *Automated bone histomorphometry using mathematical morphology*, Engineering in Medicine and Biology Society, Proceedings of the 15th Annual International Conference of the IEEE, 1993, 499–500. DOI: 10.1109/IEMBS.1993.978657.

[9] GARCÍA J.M., DOBLARÉ M., CEGOÑINO J., *Bone remodeling simulation: a tool for implant design*, Comput. Mater. Sci., 2002, Vol. 25, 100–114.

[10] GOLDSTEIN S.A., *The mechanical properties of trabecular bone: dependence on anatomic location and function*. J. Biomech., 1987, Vol. 20(11–12), 1055–1061.

[11] GONZALES R.C., WOODS R.E., *Digital image processing using Matlab*, Third edition, Prentice Hall, 2007.

[12] JANG I.G., KIM I.Y., *Computational simulation of simultaneous cortical and trabecular bone change in human proximal femur during bone remodeling*, J. Biomech., 2010, Vol. 43, 294–301.

[13] JĘDRUSIK-PAWŁOWSKA M., KROMKA-SZYDEK M., KATRA M., NIEDZIELSKA I., *Mandibular reconstruction – biomechanical strength analysis (FEM) based on a retrospective clinical analysis of selected patients*, Acta Bioeng. Biomech., 2013, Vol. 2(15), 23–31.

[14] LEKSZYCKI T., *Wybrane zagadnienia modelowania w biomechanice kości*, Instytut Podstawowych Problemów Techniki Polskiej Akademii Nauk, 2007.

[15] MALINA W., ABLAMEYKO S., PAWLAK., *Podstawy cyfrowego przetwarzania obrazów*, Akademicka Oficyna Wydawnicza EXIT, 2002.

[16] MULVIHILL B.M., PRENDERGAST P.J., *Mechanobiological regulation of the remodelling cycle in trabecular bone and possible biomechanical pathways for osteoporosis*, Clin. Biomech., 2010, Vol. 25(5), 491–498.

[17] NIKODEM A., *Correlations between structural and mechanical properties of human trabecular femur bone*, Acta Bioeng. Biomech., 2012, Vol. 2(14), 37–46.

[18] ODGAARD A., *Three-dimensional methods for quantification of cancellous bone architecture*, Bone, 1997, Vol. 20, 315–328.

[19] OTSU N., *A threshold selection method from gray-level histograms*, IEEE Trans. SMC, 1979, Vol. 1, 62–66.

[20] POCHRZĄST M., BASIAGA M., MARCINIAK J., KACZMAREK M., *Biomechanical analysis of limited-contact plate used for osteosyntesis*, Acta Bioeng. Biomech., 2014, Vol. 1(16), 99–105.

[21] ŚCIGAŁA K., *Simulation of cancellous formation and remodeling*, Division of Biomechanical Engineering and Experimental Mechanics, 2007, 1.

[22] TSUBOTA K., ADACHI T., TOMITA Y., *Functional adaptation of cancellous bone in human proximal femur predicted by trabecular surface remodeling simulation toward uniform stress state*, J. Biomech., 2002, Vol. 35, 1541–1551.

[23] TSUBOTA K., SUZUKI Y., YAMADA T., HOJO M., MAKINOUCHI A., ADACHI T., *Computer simulation of trabecular remodeling in human proximal femur using lerge-scale voxel FE models: Approach to understanding Wolff's law*, J. Biomech., 2009, Vol. 42, 1088–1094.

[24] WAKAMATSU E., SISSONS H.A., *The Cancellous bone of the Iliac Crest*, Calcif Tissue (Research) Int., 1969, Vol. 4, 147–161.

[25] WEI LI, LIN D., QING LI, SWAIN M., *Monitoring Natural Frequency for Osseointegration and Bone Remodeling Induced by Dental Implants*, International Conference on Computational Intelligence for Measurement Systems and Applications, 2009, 223–225. DOI: 10.1109/CIMSA.2009.5069953.

[26] VOKES M.S., CARPENTER A.E., *Using Cell Profiler for Automatic Identification and Measurement of Biological Objects in Images*, Curr. Protoc. Mol. Biol., 2008. DOI: 10.1002/0471142727.mb1417s82.

[27] WRONA A., *Wpływ czynników biologicznych na proces przebudowy tkanki kostnej gąbczaste*, Dokonania Naukowe doktorantów. T.1, Nauki przyrodnicze, 2013, 50–57.

[28] WRONA A., *Komputerowy Algorytm badania procesu przebudowy tkanki kostnej gąbczaste*, Acta Bio.-Opt. Inform. Med., 2014, 20, 1–10.